Kinetics of Heterogeneous Reaction of $CaCO_3$ Particles with Gaseous HNO_3 over a Wide Range of Humidity

Y. Liu,[†] E.R. Gibson,[‡] J.P. Cain,[§] H. Wang,[§] V.H. Grassian,*[,‡] and A. Laskin*[,†]

William R. Wiley Environmental Molecular Sciences Laboratory, Pacific Northwest National Laboratory, P. O. Box 999, MSIN K8-88, Richland, Washington 99352, Department of Chemistry, University of Iowa, Iowa City, Iowa 52242, and Department of Aerospace and Mechanical Engineering, University of Southern California, Los Angeles, California 90089-1453

Received: August 2, 2007; In Final Form: October 13, 2007

Heterogeneous reaction kinetics of gaseous nitric acid (HNO_3) with calcium carbonate ($CaCO_3$) particles was investigated using a particle-on-substrate stagnation flow reactor (PS-SFR). This technique utilizes the exposure of substrate deposited, isolated, and narrowly dispersed particles to a gas mixture of $HNO_3/H_2O/N_2$, followed by microanalysis of individual reacted particles using computer-controlled scanning electron microscopy with energy-dispersive X-ray analysis (CCSEM/EDX). The first series of experiments were conducted at atmospheric pressure, room temperature and constant relative humidity (40%) with a median dry particle diameter of $\bar{D}_p = 0.85\ \mu m$, particle loading densities $2 \times 10^4 \le N_s \le 6 \times 10^6\ cm^{-2}$ and free stream HNO_3 concentrations of 7, 14, and 25 ppb. The apparent, pseudo first-order rate constant for the reaction was determined from oxygen enrichment in individual particles as a function of particle loading. Quantitative treatment of the data using a diffusion-kinetic model yields a lower limit to the net reaction probability $\gamma_{net} \ge 0.06$ ($\times 3/\div 2$). In a second series of experiments, HNO_3 uptake on $CaCO_3$ particles of the same size was examined over a wide range of relative humidity, from 10 to 80%. The net reaction probability was found to increase with increasing relative humidity, from $\gamma_{net} \ge 0.003$ at RH = 10% to 0.21 at 80%.

Introduction

Mineral dust aerosol comprises one of the largest mass fractions of the total global aerosol loading. The annual production of mineral dust is estimated to be 800−2000 Tg.[1,2] As mineral dust aerosol is entrained and transported through the atmosphere, it can alter the chemical balance of the atmosphere through heterogeneous reactions with trace atmospheric gases.[3,4] Mineral dust also affects climate through direct and indirect radiative forcing.[5−7] Likewise, mineral dust particles are expected to undergo changes in their chemical composition and physical properties as a result of heterogeneous processing. Thus, when quantifying the impact of mineral dust on atmospheric chemistry and climate, it is important to consider changes in the physicochemical properties of particles as they are transported and aged in the atmosphere.[8,9]

The carbonate components of mineral dust, e.g., calcite ($CaCO_3$) and dolomite ($CaMg(CO_3)_2$), can comprise as much as 30% of the total dust loading and are known to be especially reactive with nitrogen oxides.[10] In particular, a strong correlation between Ca^{2+} and NO_3^- has been reported in a number of field and modeling studies.[11−13] Single-particle analyses of mineral dust samples have shown that as $CaCO_3$ particles are transported throughout the troposphere they can be completely converted to $Ca(NO_3)_2$.[14,15] One pathway through which this transformation can occur is through heterogeneous reaction with HNO_3:

$$CaCO_3(s) + 2HNO_3(g) \xrightarrow{\%\ RH} Ca(NO_3)_2(s,aq) + H_2CO_3(aq) \rightarrow Ca(NO_3)_2(s,aq) + CO_2(g) + H_2O \quad (1)$$

The formation of $Ca(NO_3)_2$ by reaction 1 has been observed for both pure calcium carbonate and authentic mineral dust in previous laboratory studies.[17−19]

Uptake of HNO_3 on mineral dust is one of the most important, but least certain, parameters in the analysis of the impact of dust on tropospheric ozone concentrations.[2,3,20] To assess this impact, accurate measurements of the heterogeneous uptake coefficient (γ) under conditions representative of the atmosphere are critical. Currently, most of the kinetic studies for reaction 1 have been conducted in Knudsen cell reactors under dry conditions. Under dry conditions, the reaction proceeds until the carbonate surface is saturated by nitrate, thus preventing further HNO_3 uptake.[16] For moist air, however, surface passivation is no longer an issue. The nitrate product that forms on the carbonate surface is aqueous under typical atmospheric conditions of 20−90% relative humidity (RH), facilitating continuous reaction until the entire carbonate content of a particle is consumed. Table 1 summarizes the reaction probabilities reported to date.[16,21−23] As seen, discrepancies in the uptake coefficient span several orders of magnitude, from 0.00025 to 0.1. With the exception of one study,[24] all of the uptake coefficients were observed under dry or nearly dry conditions. Based on single particle analyses, Johnson et al.[16] predicted that under typical atmospheric conditions of 20−90% RH the uptake of HNO_3 on $CaCO_3$ could be a factor

* Authors to whom correspondence should be addressed. V.H.G.: E-mail: vicki-grassian@uiowa.edu. Phone: (319) 335-1392. Fax: (319) 335-1270. A.L.: E-mail: Alexander.Laskin@pnl.gov. Phone: (509) 376-8741. Fax: (509) 376-6066.

[†] Pacific Northwest National Laboratory.

[‡] University of Iowa.

[§] University of Southern California.

10.1021/jp076169h CCC: $40.75 © 2008 American Chemical Society
Published on Web 01/31/2008

TABLE 1: Reactive Uptake Coefficients Reported for HNO_3(g) onto $CaCO_3$ and ATD at Room Temperature

type of sample	experimental technique	particle diameter, D_p (μm)	[HNO_3] ($\times 10^{-12}$ cm^{-3})	RH (%)	uptake coefficient, γ_{net}	ref
$CaCO_3$[a]	KCR−MS[b]	5−100	0.01−10	0	$(10 \pm 2) \times 10^{-2}$	21
$CaCO_3$[a]	KCR−MS	3.5	1.3	0	$(2.5 \pm 0.1) \times 10^{-4}$	22
$CaCO_3$[a]	KCR−MS	1.8	0.065	0	1.4×10^{-5}	38
$CaCO_3$[a]	KCR−MS	<10	0.065−1.3	0	$(10 \pm 2.5) \times 10^{-2}$ $(18 \pm 4.5) \times 10^{-2}$[c]	23
$CaCO_3$[a,d]	KCR−MS	0.2−10	19	0	$(2 \pm 1) \times 10^{-3}$	16
$CaCO_3$[d]	FR−N^{13} isotope tracer[e]	0.01−0.7 ($\bar{D}_p = 0.042$)	1	33	0.11	24
ATD[d]	FR−N^{13} isotope tracer[e]	0.02−0.7 ($\bar{D}_p = 0.21$)	1	12	0.022 ± 0.007	24
				20	0.03 ± 0.008	
				36	0.034 ± 0.011	
				47	0.058 ± 0.009	
				58	0.08 ± 0.012	
				66	0.072 ± 0.019	
				73	0.113 ± 0.017	
$CaCO_3$[d]	PS−SFR CCSEM/EDX[f]	0.85 ± 0.18	0.17−0.73	10	0.0032	this work
				20	0.014	
				30	0.019	
				40	0.06	
				50	0.07	
				60	0.10	
				70	0.13	
				80	0.21	

[a] Powder sample. [b] Knudsen cell reactor - mass spectrometer. [c] Values corresponding to heated and unheated $CaCO_3$. [d] Aerosol or single particle layers samples. [e] Flow reactor - ^{13}N-labeled nitric acid. [f] Particles-on-substrate stagnation flow reactor - computer-controlled scanning electron microscopy with energy-dispersed analysis of X-ray (see text).

of 10−100 faster than under dry conditions. This prediction appears to be supported by a measurement made at 33% RH, where $\gamma = 0.11$,[24] a value that is several orders of magnitude greater than those observed under dry conditions.[9,25−27] To date no systematic studies are available to provide definitive and quantitative characterization of HNO_3 uptake on $CaCO_3$ particles under a wide range of humidity.

The objective of the present work was to systematically investigate the kinetics of the heterogeneous uptake of nitric acid on calcium carbonate particles over a wide range of relative humidity. Measurements were made using a recently developed technique, which was successfully employed to study the reaction kinetics for the uptake of hydroxyl radicals and nitric acid on NaCl particles.[28,29] In this technique, particle composition changes are followed by computer-controlled scanning electron microscopy and energy dispersive X-ray analysis (CCSEM/EDX) of individual particles before and after reaction.[28,29]

Experimental Section

Materials and Sample Preparation. $CaCO_3$ particles were generated by atomizing a water suspension of calcium carbonate powder (Alfa Aesar, 99.95% purity). The particles were dried in a diffusion drier (TSI, Inc., model 3062) prior to sizing and substrate deposition using a micro-orifice uniform deposition impactor (MOUDI; model 110, MSP, Inc.). For this study, we used the fifth stage of the MOUDI to generate dry particles. These particles were deposited on filmed substrates (Carbon Type-B, 400 mesh nickel grids, Electron Microscopy Sciences, Inc.) mounted on the impaction plate. The size uniformity of substrate deposited particles was confirmed by CCSEM analysis of over 3000 particles in several samples. Figure 1 shows an SEM image of a typical $CaCO_3$ particle sample and its diameter distribution obtained from equivalent circle diameters of two-dimensional projected areas. The size distribution is log-normal with a median diameter $\bar{D}_p = 0.85$ μm and geometric standard deviation $\sigma = 1.45$. Similarly, samples of size-selected calcium nitrate particles were prepared using MOUDI for reference measurements. The $Ca(NO_3)_2$ aerosol was atomized from a 0.5 M calcium nitrate aqueous solution.

Particle Exposure Apparatus. A schematic description of the Particle-on-Substrate Stagnation Flow Reactor (PS-SFR) is shown in Figure 2. A detailed description of the apparatus and its operation have been given elsewhere.[29] Briefly, a laminar flow of premixed $N_2/H_2O/HNO_3$ gases impinges onto substrate-deposited particles. In each experiment, a substrate is loaded with $CaCO_3$ particles of a known number density (N_s) and placed atop a cylindrical Teflon sample holder 1″ in diameter. The particle sample and the holder were placed inside a sealed boro-silicate glass chamber with a FETFE O-ring quick seal. The nickel-based grid was fixed in place using a magnet embedded inside the holder.

The reactor and its gas delivery lines were made of glass and Teflon parts; neither material reacts with the HNO_3 vapor. Nitrogen was used as a carrier gas and allowed to flow through two bubblers containing a solution of concentrated HNO_3 and distilled water to generate nitric acid and water vapor, respectively. Flow rates of the reactant $HNO_3/H_2O/N_2$ mixture were controlled by three mass flow controllers and relative humidity was monitored by an inline sensor (Honeywell, inc., model HIH4000). A rotameter was installed downstream of the reactor to ensure no negative flow (into the apparatus) or leaks. A chemiluminescence NO_y analyzer (Thermo Environmental, Inc., model 42C-Y) was used to determine HNO_3 concentration exiting the reactor. Throughout this work, the reactor was passivated before each experiment for at least 2 h with a flow of the $HNO_3/H_2O/N_2$ mixture to ensure there was no significant loss of HNO_3 on the walls of the apparatus and its gas lines. During the reaction, both the HNO_3 concentration and RH were monitored continuously with fluctuations found to be smaller than 5 and 1%, respectively.

The gaseous reactant mixture is ejected at a volumetric rate of 2 L/min (STP) from a 1.25 cm diameter (outer) boro-silicate glass tube (inside diameter 0.8 cm). The flow impinges upon particles deposited on a single grid with its center placed along the flow tube centerline. The distance between the tube exit

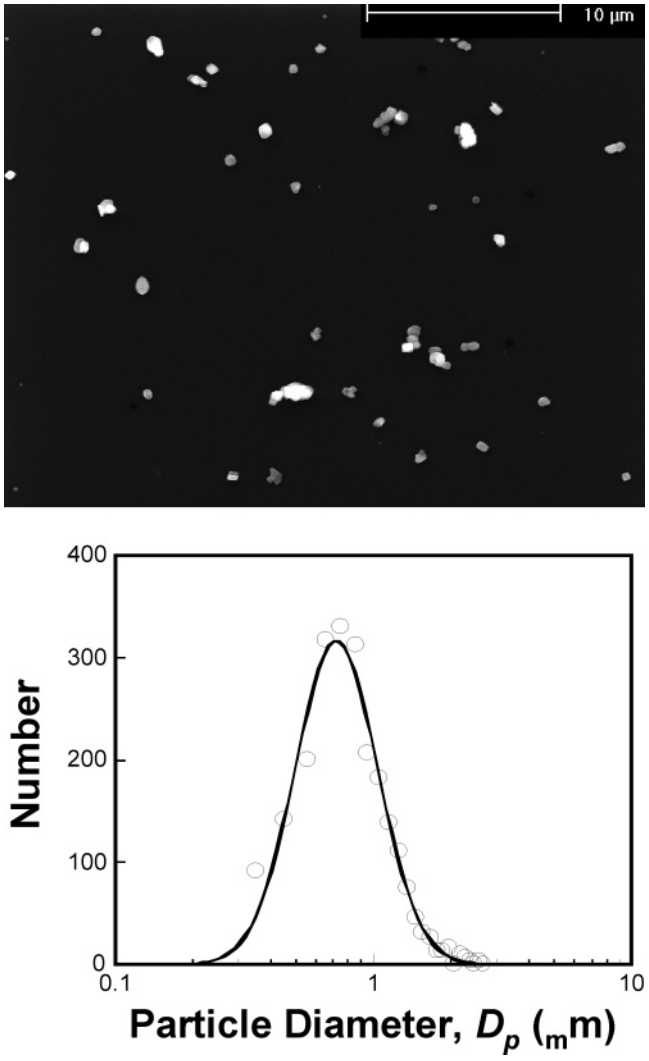

Figure 1. SEM image (top panel) and CCSEM measured particle size distribution (symbols in the bottom panel) of a typical $CaCO_3$ sample. The size distribution is fit by a log-normal distribution (solid line).

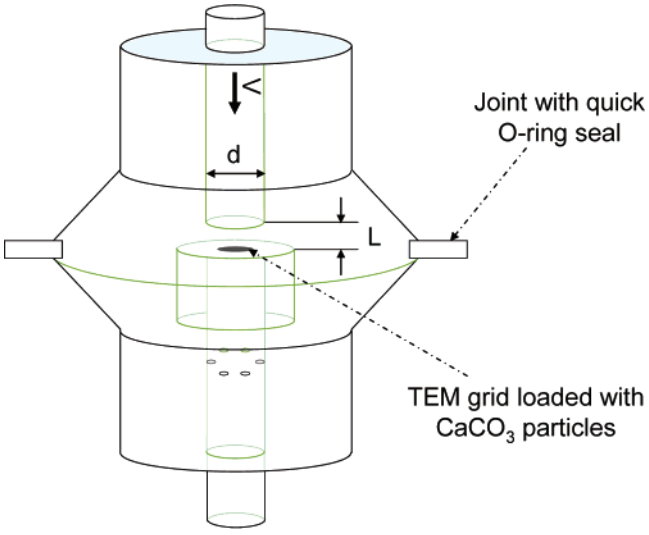

Figure 2. Schematic of the PS-SFR used in these studies for exposure of $CaCO_3$ to nitric acid vapor.

and the grid surface is 0.2 cm. These reactor parameters were chosen on the basis of computational fluid dynamics (CFD) modeling to ensure that all particles deposited on and across the grid are exposed to the same flux of HNO_3.[29] The experiments were conducted at ambient temperature and under atmospheric pressure.

CCSEM/EDX Single-Particle Analysis. Computer-controlled scanning electron microscopy coupled with energy-dispersed X-ray spectrometry was used to determine the elemental composition and loading density of $CaCO_3$ particles. The instrument used in this study is an FEI XL30 digital field emission gun environmental SEM. The microscope is equipped with an EDAX spectrometer (model PV7761/54 ME, EDAX, Inc.) that has an Si(Li) detector of 30 mm^2 in active area and an ATW2 window. The spectrometer allows X-ray detection from elements higher than beryllium ($Z > 4$). The system is equipped with *Genesis* hardware and software (EDAX, Inc.) for CCSEM/EDX single particle analysis. Particles were recognized by an increase in the detector signal above a threshold value. The program acquires an X-ray spectrum from each particle detected. Particle imaging was done by acquiring a mixed signal of backscattered (BSE) and transmitted (TE) electrons.[30] During the X-ray acquisition, the electron beam scanned over the particle projection area. The spectra were acquired for 10 s at a beam current of ~500 pA and an accelerating voltage of 20 kV. For quantification of the EDX results, the *Genesis* software utilizes a standardless microanalysis method that relates X-ray intensities to elemental concentrations through theoretically calculated equivalent intensities of corresponding peaks. Details of the quantification method can be found elsewhere.[31]

As shown in our previous work,[19] the apparent elemental composition of $CaCO_3$ and $Ca(NO_3)_2$ particles in terms of O/Ca atomic ratios measured by CCSEM/EDX analysis do not match their stoichiometric values. This instrumental response is due to a combination of atomic number, absorption and florescence (ZAF) effects, and beam damage that affect quantitation of X-ray spectra. As a result, the O/Ca ratio in $CaCO_3$ particles increases monotonically with decreasing particle size. For example, the O/C ratio was measured to be 3 and 1.3 for particles ~0.1 and ~1.0 μm in size, respectively. Additionally, the O/Ca ratio characteristic of $Ca(NO_3)_2$ particles show a rise-then-fall behavior with respect to particle size. The maximum value is ~3.5 for particles in the 0.8 to 2.0 μm size range.[19] As will be shown below, two reference values of atomic O/Ca ratios measured in the standard samples of $CaCO_3$ and $Ca(NO_3)_2$ particles are used to calculate the extent of $CaCO_3$-to-$Ca(NO_3)_2$ conversion. A larger difference in the two O/Ca reference values introduces a smaller uncertainty in our analysis. As these two O/Ca reference values have the maximum difference near 1 μm,[19] we used only one $CaCO_3$ particle size ($\bar{D}_p = 0.85$ μm, $\sigma = 1.45$) over the course of this study.

Experimental Protocol. The change in the O/Ca molar ratio of reacted particles was taken to quantify the kinetic conversion of $CaCO_3$ to $Ca(NO_3)_2$, according to reaction 1. Unlike a previous study,[29] two reference values, corresponding to 0% and 100% conversion of the initial $CaCO_3$ particles, had to be used for determining the reaction extent. The $CaCO_3$ reactant concentration upon a finite exposure time t is given by

$$\frac{[CaCO_3]_t}{[CaCO_3]_{t=0}} = \frac{[O/Ca]^{EDX}_{Ca(NO_3)_2} - [O/Ca]^{EDX}_t}{[O/Ca]^{EDX}_{Ca(NO_3)_2} - [O/Ca]^{EDX}_{CaCO_3}} \quad (2)$$

Here, $[O/Ca]^{EDX}_{CaCO_3}$ is the molar ratio of O to Ca measured for pure, unreacted $CaCO_3$ particles. The determination of $[O/Ca]_{Ca(NO_3)_2}$ requires special sample preparation due to an enhancement of the O/Ca ratio in the $Ca(NO_3)_2$ particles that results from the following reason. Once deliquesced, $Ca(NO_3)_2$ particles

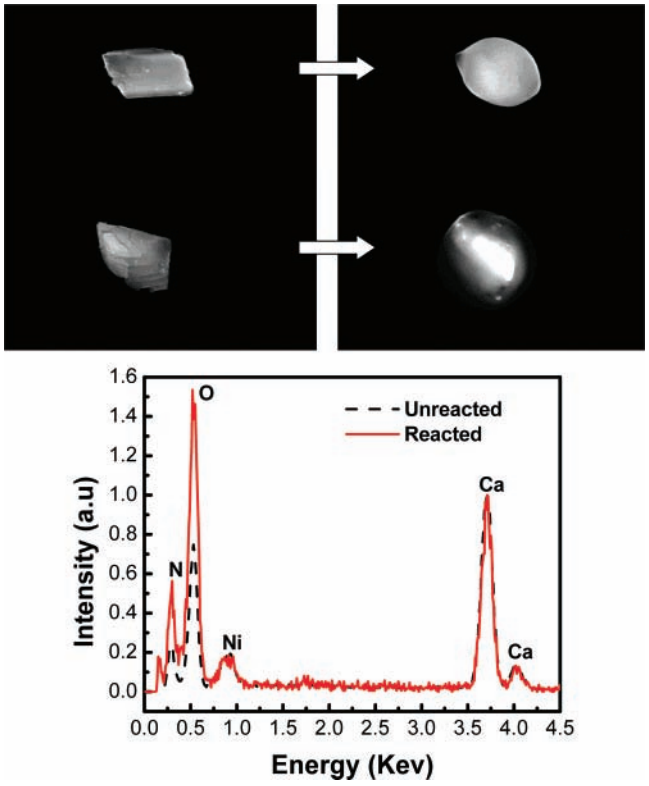

Figure 3. Top panel: SEM images of $CaCO_3$ particles before (left) and after (right) reaction with gaseous HNO_3 of 7 ppb concentration, 40% RH and reaction time of 120 min. Bottom panel: typical EDX spectra of $CaCO_3$ particles before and after reaction.

always retain some water and do not dry out completely even under vacuum conditions.[32,33] A recent study showed that the amount of HNO_3 uptake was greater than that expected for known nitrate solubility suggesting $Ca(NO_3)_2$ itself could irreversibly take up HNO_3.[34] These considerations led us to determine the reference value for $[O/Ca]_{Ca(NO_3)_2}$ by exposing $Ca(NO_3)_2$ particles to a stream of $HNO_3/H_2O/N_2$ identical to the actual kinetic experiments for several hours. The resulting particles were taken for $[O/Ca]_{Ca(NO_3)_2}$ determination by EDX. Indeed, $Ca(NO_3)_2$ particles treated in this manner displayed O/Ca ratios nearly a factor of 1.2 higher than that of untreated $Ca(NO_3)_2$ particles. We assume that the O/Ca ratio varies linearly between the two reference values as the reaction proceeds. This assumption is supported by the fact that the interaction volume of the 20 kV electron beam applied in the $CaCO_3/Ca(NO_3)_2$ media is much larger than 1 μm^3, i.e., the volume of particles studied in this work. Therefore, the corresponding X-ray spectra reflect an averaged composition of all the particles.

In principle, measurements made for the N/Ca ratio could be also used to determine the reaction extent.[29] However, the quantitative detection of nitrogen is typically less accurate because of complications due to a deep gap in the transmission characteristic of the ATW2 window that overlaps the Kα line of nitrogen. This results in very low intensities of the nitrogen peak measured by EDX, and consequently, in difficulties in its accurate deconvolution.

The top panel of Figure 3 shows typical SEM images of $CaCO_3$ particles before and after exposure to gaseous HNO_3. The change observed in the morphology of individual particles is consistent with previous observations,[18] indicating the reactive transformation from crystalline $CaCO_3$ to amorphous $Ca(NO_3)_2$ particles. A comparison of the accompanying EDX spectra (the bottom panel of Figure 3) reveals an enhancement of oxygen and nitrogen content in the particles after reactive exposure, as one would expect from the stoichiometry of reaction 1.

As shown in Table 2, three sets of data were obtained for the first series of experiments (A, B, and C). Each set used a fixed HNO_3 free-stream concentration (A, 7.1 ± 0.4; B, 14.4 ± 0.7; and C, 24.5 ± 1.5 ppb) at RH = 40% over a wide range of reaction times (t = 5 to 300 min) and particle loading densities ($N_s = 2 \times 10^4$ to 6×10^6 cm^{-2}). The HNO_3 concentrations used in the first set of experiments correspond to 10 to 20 ppb levels that are found in polluted environments.[35] Altogether, over 100 substrates containing $CaCO_3$ particles were analyzed over the course of this study. A vast majority of the particles had less than a 0.35 $Ca(NO_3)_2/CaCO_3$ conversion ratio. An additional series of experiments (data set labeled D) were carried out to investigate the effect of relative humidity on the reactive uptake of HNO_3 on $CaCO_3$. These data are given in Table 3.

The kinetics data were analyzed using a theoretical kinetics-diffusion model of gaseous reactant transport from the bulk gas to the substrate surface.[28] The effects of diffusion arise from the finite proximity of the reacting particles mounted on the substrate at high particle loadings, which alter the effective local concentrations of the gaseous reactant (HNO_3) immediately above the particle surface and hence the apparent kinetics of the $CaCO_3$-to-$Ca(NO_3)_2$ conversion. For series A, B, and C experiments, the influence of particle loading was eliminated by fitting the kinetic data as a function of particles density N_s using a diffusion-kinetic analysis,[28,29] as will be presented in the Discussion section. Experiments in series D were done using a smaller particle loading ($N_s < 5 \times 10^4$ cm^{-2}) to ensure that the measured kinetics are representative of the single particle interacting with the gas phase.[28,29] Even under this condition, the reaction rate may be inherently limited by gas diffusion because the particle size is larger than the mean free path of the gas.

Results and Discussion

Rate Constant and Net Uptake Coefficient. As shown in eq 2, the change in the O/Ca ratio in reacted particles was taken to measure the extent of $CaCO_3$-to-$Ca(NO_3)_2$ conversion. It is important to note that carbonic acid (H_2CO_3), an intermediate of reaction 1, is unstable and decomposes to water and carbon dioxide,[36] both of which for the most part degas as reacted particles are subject to vacuum condition during microscopy analysis. Because of the stoichiometry of reaction 1, the change in the O/Ca ratio determined for vacuum-dried, reacted particles is equal to the reaction extent given by eq 2, and the reaction kinetics may be expressed accordingly,

$$-\frac{d[CaCO_3]}{dt} = k_I[CaCO_3] \quad (3)$$

where $[CaCO_3]$ represents the concentration of $CaCO_3$ in the particles, and k_I is the apparent, pseudo first-order rate constant. If k_I is a constant during the course of the reaction, its value may be calculated from

$$k_I = -\frac{1}{t}\ln\left(\frac{[CaCO_3]_t}{[CaCO_3]_{t=0}}\right) = -\frac{1}{t}\ln\left(\frac{[O/Ca]^{EDX}_{Ca(NO_3)_2} - [O/Ca]^{EDX}_t}{[O/Ca]^{EDX}_{Ca(NO_3)_2} - [O/Ca]^{EDX}_{CaCO_3}}\right) \quad (4)$$

TABLE 2: Summary of Experimental Conditions and Pseudo First-Order Rate Constants[a]

$[HNO_3]_\infty$ (ppb)	$N_s \times 10^{-5}$ (cm^{-2})	Time, t (min)	$[O/Ca]^{EDX}_{CaCO_3,t}$	$[O/Ca]^{EDX}_{CaCO_3,t=0}$	$[O/Ca]^{EDX}_{Ca(NO_3)_2}$	$k_I \times 10^4$ (s^{-1})
Series A: RH = 40%; $\bar{D}_p = 0.85 \pm 0.18$ μm; $[HNO_3]_\infty = 24.5 \pm 1.5$ ppb						
27.0	2.4 ± 0.6	10	2.92 ± 0.86	2.04 ± 0.49	4.58 ± 0.90	7.1 (×2.2/÷2.2)
27.0	4.0 ± 1.0	10	2.98 ± 0.90	2.04 ± 0.49	4.58 ± 0.90	7.7 (×2.3/÷2.3)
22.0	2.7 ± 0.7	10	2.67 ± 0.83	2.04 ± 0.49	4.58 ± 0.90	4.7 (×2.5/÷2.0)
22.0	2.4 ± 0.6	10	2.71 ± 0.75	2.04 ± 0.49	4.58 ± 0.90	5.1 (×2.3/÷2.1)
21.0	3.8 ± 1.0	10	2.51 ± 0.79	2.04 ± 0.49	4.58 ± 0.90	3.4 (×2.8/÷2.0)
21.0	3.6 ± 0.9	10	2.60 ± 0.94	2.04 ± 0.49	4.58 ± 0.90	4.1 (×2.8/÷2.0)
21.0	0.6 ± 0.1	5	2.58 ± 1.24	2.04 ± 0.49	4.58 ± 0.90	8.1 (×3.5/÷2.0)
21.0	0.4 ± 0.1	5	2.57 ± 0.92	2.04 ± 0.49	4.58 ± 0.90	7.9 (×2.9/÷2.0)
23.0	0.6 ± 0.1	10	2.70 ± 0.95	2.04 ± 0.49	4.58 ± 0.90	5.0 (×2.6/÷2.0)
23.0	0.6 ± 0.1	10	2.86 ± 1.17	2.04 ± 0.49	4.58 ± 0.90	6.5 (×2.8/÷2.0)
26.5	4.9 ± 1.0	10	2.85 ± 1.23	2.36 ± 0.56	5.67 ± 1.00	2.7 (×3.5/÷2.0)
26.5	4.5 ± 1.1	10	3.06 ± 1.26	2.36 ± 0.56	5.67 ± 1.00	3.9 (×2.9/÷2.0)
26.0	8.7 ± 2.2	12	2.73 ± 0.87	2.36 ± 0.56	5.67 ± 1.00	1.6 (×3.3/÷2.0)
26.0	7.7 ± 1.9	12	2.88 ± 1.14	2.36 ± 0.56	5.67 ± 1.00	2.3 (×3.2/÷2.0)
25.1	6.3 ± 1.6	13	2.68 ± 0.93	2.36 ± 0.56	5.67 ± 1.00	1.3 (×3.8/÷2.0)
25.1	9.6 ± 2.4	13	2.90 ± 1.21	2.36 ± 0.56	5.67 ± 1.00	2.3 (×3.2/÷2.0)
25.2	3.8 ± 0.9	9	3.35 ± 1.31	2.36 ± 0.56	5.67 ± 1.00	6.6 (×2.5/÷2.0)
25.2	3.1 ± 0.8	9	3.23 ± 1.23	2.36 ± 0.56	5.67 ± 1.00	5.6 (×2.6/÷2.0)
24.7	2.4 ± 0.6	8	3.27 ± 1.25	2.36 ± 0.56	5.67 ± 1.00	6.7 (×2.5/÷2.0)
24.7	2.1 ± 0.5	8	3.20 ± 1.29	2.36 ± 0.56	5.67 ± 1.00	6.1 (×2.7/÷2.0)
24.2	2.6 ± 0.7	6.5	2.69 ± 0.88	2.36 ± 0.56	5.67 ± 1.00	2.7 (×3.6/÷2.0)
24.2	2.2 ± 0.6	6.5	2.97 ± 1.10	2.36 ± 0.56	5.67 ± 1.00	5.2 (×2.8/÷2.0)
24.0	0.3 ± 0.1	5	3.23 ± 1.24	2.36 ± 0.56	5.67 ± 1.00	10.1 (×2.6/÷2.0)
25.0	0.3 ± 0.1	5	3.62 ± 1.26	2.36 ± 0.56	5.67 ± 1.00	15.9 (×2.3/÷2.3)
25.0	0.5 ± 0.1	5	3.67 ± 1.27	2.36 ± 0.56	5.67 ± 1.00	16.7 (×2.6/÷2.0)
23.8	0.2 ± 0.1	5	3.35 ± 1.39	2.36 ± 0.56	5.67 ± 1.00	11.8 (×2.6/÷2.0)
23.9	0.9 ± 0.2	5	2.54 ± 0.57	2.14 ± 0.38	5.67 ± 1.00	4.0 (×2.3/÷2.0)
23.9	1.4 ± 0.3	5	2.48 ± 0.74	2.14 ± 0.38	5.67 ± 1.00	3.4 (×2.9/÷2.0)
24.2	1.5 ± 0.4	6	3.15 ± 1.37	2.14 ± 0.38	5.67 ± 1.00	9.4 (×2.5/÷2.0)
24.2	1.3 ± 0.3	6	2.84 ± 0.93	2.14 ± 0.38	5.67 ± 1.00	6.1 (×2.3/÷2.0)
26.5	1.4 ± 0.4	5.5	2.53 ± 0.57	2.14 ± 0.38	5.67 ± 1.00	3.5 (×2.4/÷2.0)
26.5	1.4 ± 0.4	5.5	2.53 ± 0.69	2.14 ± 0.38	5.67 ± 1.00	3.5 (×2.6/÷2.0)
26.1	1.7 ± 0.4	6.5	2.96 ± 1.02	2.14 ± 0.38	5.67 ± 1.00	6.8 (×2.2/÷2.1)
25.0	30.3 ± 7.6	25	2.53 ± 0.85	2.27 ± 0.72	5.67 ± 1.00	0.5 (×4.4/÷2.0)
27.0	27.8 ± 6.9	30	2.75 ± 1.12	2.27 ± 0.72	5.67 ± 1.00	0.8 (×3.4/÷2.0)
27.0	35.7 ± 8.9	30	2.67 ± 1.24	2.27 ± 0.72	5.67 ± 1.00	0.7 (×4.1/÷2.0)
24.2	1.0 ± 0.3	5	2.96 ± 1.28	2.36 ± 0.56	5.67 ± 1.00	6.7 (×3.1/÷2.0)
24.2	0.8 ± 0.2	5	3.34 ± 1.58	2.36 ± 0.56	5.67 ± 1.00	11.6 (×2.9/÷2.0)
Series B: RH = 40%; $\bar{D}_p = 0.85 \pm 0.18$ μm; $[HNO_3]_\infty = 14.4 \pm 0.7$ ppb						
15.5	1.1 ± 0.3	14	2.97 ± 1.70	2.22 ± 0.91	5.51 ± 1.03	3.1 (×3.8/÷2.0)
15.5	1.0 ± 0.3	14	2.97 ± 1.55	2.22 ± 0.91	5.51 ± 1.03	3.1 (×3.5/÷2.0)
13.7	0.8 ± 0.2	14.5	3.39 ± 1.68	2.22 ± 0.91	5.51 ± 1.03	5.1 (×3.1/÷2.0)
13.7	0.9 ± 0.2	14.5	3.51 ± 1.49	2.22 ± 0.91	5.51 ± 1.03	5.7 (×2.7/÷2.1)
15.0	5.8 ± 1.5	45	3.23 ± 1.49	2.24 ± 0.99	5.51 ± 1.03	1.3 (×3.0/÷2.0)
15.0	2.3 ± 0.6	45	3.19 ± 1.18	2.24 ± 0.99	5.51 ± 1.03	1.3 (×2.6/÷2.0)
14.5	10.8 ± 2.7	45	2.58 ± 1.29	2.24 ± 0.99	5.51 ± 1.03	0.4 (×5.2/÷2.0)
14.0	3.8 ± 0.9	46	3.24 ± 1.55	2.24 ± 0.99	5.51 ± 1.03	1.3 (×3.1/÷2.0)
14.0	1.8 ± 0.5	46	3.15 ± 1.60	2.24 ± 0.99	5.51 ± 1.03	1.2 (×3.3/÷2.0)
13.8	0.2 ± 0.1	14.5	3.38 ± 2.02	2.22 ± 0.91	5.51 ± 1.03	5.0 (×3.8/÷2.0)
14.1	0.4 ± 0.1	16	3.26 ± 1.02	2.22 ± 0.91	5.51 ± 1.03	4.0 (×2.3/÷2.2)
14.9	55.1 ± 13.8	67	2.49 ± 1.24	2.24 ± 0.96	5.51 ± 1.03	0.2 (×6.4/÷2.0)
14.9	51.8 ± 13.0	67	2.48 ± 1.03	2.24 ± 0.96	5.51 ± 1.03	0.2 (×5.0/÷2.0)
14.4	42.9 ± 10.7	85	2.54 ± 1.23	2.24 ± 0.96	5.51 ± 1.03	0.2 (×5.5/÷2.0)
14.7	7.8 ± 2.0	60	2.74 ± 1.23	2.24 ± 0.99	5.51 ± 1.03	0.5 (×3.8/÷2.0)
14.7	6.1 ± 1.5	60	2.83 ± 1.25	2.24 ± 0.99	5.51 ± 1.03	0.6 (×3.4/÷2.0)
14.7	5.1 ± 1.3	60	3.10 ± 1.43	2.24 ± 0.99	5.51 ± 1.03	0.9 (×3.1/÷2.0)
14.2	0.3 ± 0.1	12	3.08 ± 1.01	2.22 ± 0.91	5.51 ± 1.03	4.2 (×2.5/÷2.0)
14.2	0.3 ± 0.1	12	3.09 ± 1.35	2.22 ± 0.91	5.51 ± 1.03	4.3 (×2.9/÷2.0)
13.2	0.5 ± 0.1	12	2.77 ± 1.13	2.22 ± 0.91	5.51 ± 1.03	2.5 (×3.3/÷2.0)
13.2	0.6 ± 0.1	12	3.28 ± 1.56	2.22 ± 0.91	5.51 ± 1.03	5.4 (×3.0/÷2.0)
13.1	0.3 ± 0.1	9	2.97 ± 1.23	1.98 ± 0.42	5.51 ± 0.97	6.1 (×2.3/÷2.1)
15.3	0.3 ± 0.1	12	2.88 ± 1.23	1.98 ± 0.42	5.51 ± 0.97	4.1 (×2.4/÷2.0)
15.3	0.2 ± 0.1	12	3.08 ± 0.68	1.98 ± 0.42	5.51 ± 0.97	5.2 (×1.7/÷2.9)
Series C: RH = 40%; $\bar{D}_p = 0.85 \pm 0.18$ μm; $[HNO_3]_\infty = 7.1 \pm 0.4$ ppb						
6.5	2.6 ± 0.6	25	2.88 ± 1.4	2.04 ± 0.49	4.58 ± 0.90	2.7 (×3.3/÷2.0)
6.5	1.6 ± 0.4	25	2.30 ± 0.9	2.04 ± 0.49	4.58 ± 0.90	0.7 (×4.4/÷2.0)
7.0	1.8 ± 0.5	28	2.90 ± 1.4	2.04 ± 0.49	4.58 ± 0.90	2.5 (×3.3/÷2.0)
7.1	1.8 ± 0.4	23	2.65 ± 1.2	2.04 ± 0.49	4.58 ± 0.90	2.0 (×3.1/÷2.0)
7.1	2.0 ± 0.5	23	2.68 ± 1.3	2.04 ± 0.49	4.58 ± 0.90	2.1 (×3.3/÷2.0)
7.3	1.9 ± 0.5	20	2.63 ± 1.0	2.04 ± 0.49	4.58 ± 0.90	2.2 (×2.9/÷2.0)
7.3	2.6 ± 0.7	20	2.55 ± 1.1	2.04 ± 0.49	4.58 ± 0.90	1.9 (×3.3/÷2.0)
7.2	2.4 ± 0.6	23	2.32 ± 1.1	2.04 ± 0.49	4.58 ± 0.90	0.9 (×4.8/÷2.0)

TABLE 2. (Continued)

$[HNO_3]_\infty$ (ppb)	$N_s \times 10^{-5}$ (cm^{-2})	Time, t (min)	$[O/Ca]^{EDX}_{CaCO_3,t}$	$[O/Ca]^{EDX}_{CaCO_3,t=0}$	$[O/Ca]^{EDX}_{Ca(NO_3)_2}$	$k_I \times 10^4$ (s^{-1})
7.0	4.2 ± 1.1	30	2.67 ± 1.2	2.04 ± 0.49	4.58 ± 0.90	1.6 (×3.2/÷2.0)
7.0	2.8 ± 0.7	30	2.48 ± 0.9	2.04 ± 0.49	4.58 ± 0.90	1.0 (×3.1/÷2.0)
6.4	0.7 ± 0.2	30	2.32 ± 1.0	2.04 ± 0.49	4.58 ± 0.90	0.6 (×4.7/÷2.0)
6.4	0.8 ± 0.2	30	2.43 ± 1.1	2.04 ± 0.49	4.58 ± 0.90	0.9 (×3.8/÷2.0)
6.3	0.5 ± 0.1	35	2.32 ± 1.0	2.04 ± 0.49	4.58 ± 0.90	1.0 (×4.0/÷2.0)
6.3	0.6 ± 0.2	35	2.50 ± 1.3	2.04 ± 0.49	4.58 ± 0.90	2.3 (×4.0/÷2.0)
7.0	1.5 ± 0.4	23	3.12 ± 2.0	2.22 ± 0.91	5.51 ± 1.03	2.3 (×4.1/÷2.0)
7.0	1.4 ± 0.3	23	2.60 ± 1.6	2.22 ± 0.91	5.51 ± 1.03	0.9 (×5.5/÷2.0)
7.5	1.2 ± 0.3	21	2.46 ± 1.5	2.22 ± 0.91	5.51 ± 1.03	0.6 (×4.8/÷2.0)
7.5	1.1 ± 0.3	21	2.90 ± 1.8	2.22 ± 0.91	5.51 ± 1.03	1.8 (×4.3/÷2.0)
6.7	0.8 ± 0.2	23	3.02 ± 2.0	2.22 ± 0.91	5.51 ± 1.03	2.0 (×4.2/÷2.0)
6.7	0.8 ± 0.2	23	2.56 ± 1.5	2.22 ± 0.91	5.51 ± 1.03	0.9 (×5.7/÷2.0)
7.0	0.2 ± 0.1	10	2.69 ± 1.7	1.98 ± 0.42	5.51 ± 1.03	3.7 (×3.4/÷2.0)
7.0	0.2 ± 0.1	10	2.52 ± 1.1	1.98 ± 0.42	5.51 ± 1.03	2.8 (×2.9/÷2.0)
7.0	0.2 ± 0.0	10	2.45 ± 1.8	1.98 ± 0.42	5.51 ± 1.03	2.4 (×4.8/÷2.0)
6.5	0.2 ± 0.0	10	2.39 ± 0.8	1.98 ± 0.42	5.51 ± 1.03	2.1 (×2.9/÷2.0)
6.5	0.2 ± 0.0	10	2.30 ± 0.4	1.98 ± 0.42	5.51 ± 1.03	1.6 (×2.3/÷2.0)
6.2	0.1 ± 0.0	12	2.66 ± 1.5	1.98 ± 0.42	5.51 ± 1.03	3.0 (×3.3/÷2.0)
6.2	0.1 ± 0.0	12	2.71 ± 1.6	1.98 ± 0.42	5.51 ± 1.03	3.2 (×3.2/÷2.0)
7.5	0.5 ± 0.1	15	2.28 ± 1.0	1.98 ± 0.42	5.51 ± 1.03	1.0 (×3.8/÷2.0)
7.5	0.4 ± 0.1	15	2.46 ± 1.2	1.98 ± 0.42	5.51 ± 1.03	1.6 (×3.4/÷2.0)
6.8	0.5 ± 0.1	12	2.51 ± 1.2	1.98 ± 0.42	5.51 ± 1.03	2.3 (×3.1/÷2.0)
6.8	0.5 ± 0.1	12	2.28 ± 1.2	1.98 ± 0.42	5.51 ± 1.03	1.2 (×4.5/÷2.0)
7.1	7.6 ± 1.9	180	2.76 ± 1.3	1.98 ± 0.42	5.51 ± 1.03	0.2 (×2.7/÷2.0)
7.1	16.6 ± 4.2	180	2.86 ± 1.4	1.98 ± 0.42	5.51 ± 1.03	0.3 (×2.7/÷2.0)
6.9	6.2 ± 1.6	150	2.91 ± 1.4	1.98 ± 0.42	5.51 ± 1.03	0.3 (×2.7/÷2.0)
6.9	14.3 ± 3.6	150	2.82 ± 1.5	1.98 ± 0.42	5.51 ± 1.03	0.3 (×2.8/÷2.0)
7.8	0.4 ± 0.1	15	2.48 ± 0.9	1.98 ± 0.42	5.51 ± 1.03	1.7 (×2.7/÷2.0)
7.8	0.5 ± 0.1	15	2.93 ± 1.3	1.98 ± 0.42	5.51 ± 1.03	3.5 (×2.4/÷2.0)
7.5	7.0 ± 1.7	180	3.12 ± 1.5	1.98 ± 0.42	5.51 ± 1.03	0.4 (×2.5/÷2.1)
7.5	7.3 ± 1.8	180	3.22 ± 1.5	1.98 ± 0.42	5.51 ± 1.03	0.4 (×2.5/÷2.1)
7.9	4.4 ± 1.1	50	3.04 ± 1.5	1.98 ± 0.42	5.51 ± 1.03	1.2 (×2.5/÷2.0)
7.9	1.7 ± 0.4	50	3.12 ± 1.4	1.98 ± 0.42	5.51 ± 1.03	1.3 (×2.4/÷2.1)
7.4	27.8 ± 6.9	300	3.11 ± 1.6	1.98 ± 0.42	5.51 ± 1.03	0.2 (×2.6/÷2.0)
7.4	28.6 ± 7.2	300	2.56 ± 1.1	1.98 ± 0.42	5.5 ± 0.97	0.1 (×2.7/÷2.0)
7.4	26.2 ± 6.6	300	2.64 ± 1.1	1.98 ± 0.42	5.5 ± 0.97	0.1 (×2.5/÷2.0)
7.4	32.1 ± 8.0	300	2.61 ± 1.1	1.98 ± 0.42	5.5 ± 0.97	0.1 (×2.6/÷2.0)
7.2	0.4 ± 0.1	12	2.51 ± 0.9	1.98 ± 0.42	5.5 ± 0.97	2.3 (×2.6/÷2.0)
7.0	0.4 ± 0.1	12	2.44 ± 1.7	1.98 ± 0.42	5.5 ± 0.97	1.9 (×4.5/÷2.0)
7.8	0.2 ± 0.1	16	3.21 ± 1.1	1.98 ± 0.42	5.5 ± 0.97	4.5 (×2.0/÷2.4)
7.8	0.3 ± 0.1	16	2.85 ± 1.0	1.98 ± 0.42	5.5 ± 0.97	2.9 (×2.1/÷2.2)
7.8	0.3 ± 0.1	16	2.72 ± 1.2	1.98 ± 0.42	5.5 ± 0.97	2.5 (×2.6/÷2.0)

[a] Uncertainty values represent one-standard deviation. k_I is the apparent, pseudo first-order rate constant determined from eq 4, and the uncertainty factors in the parentheses correspond to one standard deviation in $[O/Ca]^{EDX}_{CaCO_3,t}$, $[O/Ca]^{EDX}_{CaCO_3,t=0}$ and $[O/Ca]^{EDX}_{Ca(NO_3)_2}$.

Table 2 lists the $[O/Ca]^{EDX}_{Ca(NO_3)_2}$, $[O/Ca]^{EDX}_t$, $[O/Ca]^{EDX}_{CaCO_3}$ and k_I values for the first series of experiments. The uncertainty of k_I was calculated from the standard deviations in the measurements of the O/Ca ratios and is expressed in Table 2 as the multiplication and division factor (i.e., the uncertainty factor) because of the logarithmic function of eq 4. To examine the validity of the pseudo first-order rates, we analyzed the $[HNO_3]_\infty/k_I$ values taken at several averaged particle loadings but over a range of reaction times ($6 \le t \le 300$ min). Here, $[HNO_3]_\infty$ is the gaseous HNO_3 concentration in the free stream. The analysis shows no discernible, systematic variation of $[HNO_3]_\infty/k_I$ as a function of time, as shown in Figure 4. That is, k_I is time invariant over the range of reaction times investigated.

Because of the finite density and thus spatial separation of the particles on the substrate, the measured pseudo first-order rate constant is influenced by diffusive competition of the gaseous reactant, and as such its value is dependent on the particle loading density. As shown in a previous diffusion-kinetic analysis,[28] k_I may be related to N_s by the following equation:

$$\frac{[HNO_3]_\infty}{k_I} = \frac{[HNO_3]_\infty}{k^*_I}(1 + \delta k_s) + bN_S \qquad (5)$$

where k^*_I is the lower limit of the apparent first-order rate constant in the limit of $N_s \rightarrow 0$, i.e., that of a single particle, k_s is the rate constant of the HNO_3 reaction with the substrate surface and δ is a parameter equal to $l/D_{HNO_3-N_2}$, where l is the boundary layer thickness above the substrate and $D_{HNO_3-N_2}$ is the HNO_3-N_2 binary diffusion coefficient. In eq 5, parameter b is related to particle volume and the characteristic diffusion length of HNO_3. Its value is approximately constant during reaction.[28] A plot of $[HNO_3]_\infty/k_I$ data versus N_s and extrapolating the data to zero N_s yields the value for k^*_I, as shown in Figure 5. The solid line in Figure 5 represents the fit, and the dashed lines represent the scatter of the data. As seen, the data cluster around the fitted line within a degree of scatter, but no systematic variation is observed as a function of the free-stream HNO_3 concentration, which again verifies the assumption of pseudo first-order reaction kinetics. The value of $[HNO_3]_\infty/k_I$ is found to be 4.8×10^{14} (×3/÷2) cm^{-3}·s in the limit of $N_s \rightarrow 0$. The uncertainty of the data and their extrapolation are represented by the dashed lines in Figure 5

An underlying assumption of the data analysis[28,29] is that the substrate is unreative, i.e., HNO_3 consumption by the substrate does not affect kinetics of the HNO_3-to-$CaCO_3$ reaction ($\delta k_s \ll 1$ in eq 5). If some of the reactive gas molecules are removed

TABLE 3: Summary of Experimental Conditions and Pseudo First-Order Rate Constants in Relative Humidity Dependency Study[a] (Series D)

$[HNO_3]_\infty$ (ppb)	$N_s \times 10^{-4}$ (cm^{-2})	time (min)	$[O/Ca]^{EDX}_{CaCO_3,t}$	$k_I \times 10^4$ (s^{-1})	$[HNO_3]_\infty$ (ppb)	$N_s \times 10^{-4}$ (cm^{-2})	time (min)	$[O/Ca]^{EDX}_{CaCO_3,t}$	$k_I \times 10^4$ (s^{-1})
				RH = 10%					
22.0	2.2 ± 0.5	25.0	2.44 ± 1.17	0.9 (×3.2/÷2.0)	22.2	2.3 ± 0.6	50.0	2.35 ± 1.00	0.4 (×3.8/÷2.0)
22.2	2.4 ± 0.6	50.0	2.36 ± 1.14	0.4 (×3.9/÷2.0)	21.6	2.4 ± 0.6	50.0	2.27 ± 1.11	0.3 (×5.1/÷2.0)
34.5	3.3 ± 0.8	50.0	2.26 ± 0.76	0.3 (×4.7/÷2.0)	34.5	3.3 ± 0.8	40.0	2.57 ± 1.26	0.8 (×2.7/÷2.0)
34.5	1.9 ± 0.5	40.0	3.07 ± 1.76	1.5 (×2.1/÷1.8)	34.5	2.5 ± 0.6	40.0	2.53 ± 1.33	0.7 (×3.0/÷2.0)
34.5	3.2 ± 0.8	40.0	2.39 ± 1.00	0.5 (×3.6/÷2.0)					
				RH = 20%					
16.2	2.2 ± 0.5	16.0	2.35 ± 1.76	1.2 (×4.5/÷2.0)	20.0	3.5 ± 0.9	16	3.11 ± 1.80	4.0 (×2.0/÷1.8)
16.2	1.7 ± 0.4	16.0	2.53 ± 1.51	1.8 (×3.0/÷2.0)	20.0	4.8 ± 1.2	16	2.61 ± 1.10	2.1 (×2.5/÷2.0)
19.5	2.5 ± 0.6	16.0	2.61 ± 1.17	2.1 (×2.5/÷2.0)	20.0	3.2 ± 0.8	16	2.37 ± 0.88	1.2 (×3.4/÷2.0)
19.5	2.2 ± 0.5	16.0	2.72 ± 1.15	2.5 (×2.2/÷2.0)	20.8	2.3 ± 0.6	16	2.38 ± 1.39	1.3 (×4.1/÷2.0)
19.5	3.5 ± 0.9	16.0	2.40 ± 0.85	1.3 (×3.3/÷2.0)	20.8	2.1 ± 0.5	16	2.85 ± 1.57	3.0 (×2.2/÷1.9)
21.0	3.2 ± 0.8	16.0	2.50 ± 1.42	1.7 (×3.1/÷2.0)					
				RH = 30%					
8.8	3.1 ± 0.8	15.0	2.43 ± 1.19	1.5 (×3.4/÷2.0)	8.2	3.7 ± 0.9	35.0	2.85 ± 1.40	1.4 (×2.2/÷1.9)
8.7	3.3 ± 0.8	15.0	2.47 ± 0.99	1.7 (×3.2/÷2.0)	8.0	1.7 ± 0.4	40.0	3.19 ± 0.82	1.8 (×1.9/÷1.7)
8.9	2.1 ± 0.5	30.0	2.37 ± 1.15	0.7 (×3.9/÷2.0)	8.0	3.7 ± 0.9	40.0	2.64 ± 1.30	0.9 (×2.5/÷2.0)
8.8	2.5 ± 0.6	30.0	2.39 ± 1.19	0.7 (×3.8/÷2.0)	8.2	4.4 ± 1.1	40.0	2.79 ± 1.25	1.1 (×2.2/÷1.9)
8.5	4.2 ± 1.0	35.0	2.67 ± 1.27	1.0 (×2.5/÷2.0)	8.2	2.2 ± 0.5	40.0	2.87 ± 0.56	1.2 (×2.0/÷1.8)
8.5	4.4 ± 1.1	35.0	2.52 ± 1.09	0.8 (×2.8/÷2.0)					
				RH = 40%					
13.8	2.2 ± 0.5	14.5	3.38 ± 2.02	5.0 (×2.0/÷1.8)	6.2	1.3 ± 0.3	12.0	2.66 ± 1.54	3.0 (×2.6/÷2.0)
14.1	3.7 ± 0.9	16.0	3.26 ± 1.02	4.0 (×2.0/÷1.8)	6.2	1.2 ± 0.3	12.0	2.71 ± 1.61	3.2 (×2.4/÷2.0)
14.2	2.7 ± 0.7	12.0	3.08 ± 1.01	4.2 (×2.2/÷1.9)	7.2	4.2 ± 1.1	12.0	2.51 ± 0.94	2.3 (×2.6/÷2.0)
14.2	2.8 ± 0.7	12.0	3.09 ± 1.35	4.3 (×2.2/÷1.9)	7.0	4.0 ± 1.0	12.0	2.44 ± 1.69	1.9 (×3.6/×f72.0)
7.0	2.0 ± 0.5	10.0	2.69 ± 1.69	3.7 (×2.6/÷2.0)	7.8	2.4 ± 0.6	16.0	3.21 ± 1.10	4.5 (×1.9/÷1.7)
7.0	2.1 ± 0.5	10.0	2.52 ± 1.12	2.8 (×2.9/÷2.0)	7.8	2.9 ± 0.7	16.0	2.85 ± 0.99	2.9 (×2.1/÷1.8)
7.0	1.7 ± 0.4	10.0	2.45 ± 1.82	2.4 (×3.8/÷2.0)	7.8	3.3 ± 0.8	16.0	2.72 ± 1.23	2.5 (×2.2/÷1.9)
6.5	1.5 ± 0.4	10.0	2.39 ± 0.84	2.1 (×3.4/÷2.0)					
				RH = 50%					
7.6	1.9 ± 0.5	9.5	2.64 ±0.92	3.6 (×2.3/÷2.0)	7.0	3.9 ± 1.0	10.0	2.43 ± 0.89	2.3 (×3.3/÷2.0)
7.6	2.1 ± 0.5	9.5	2.76 ± 0.96	4.4 (×2.2/÷1.9)	7.0	2.7 ± 0.7	10.0	2.59 ± 0.96	3.2 (×2.5/÷2.0)
7.2	1.7 ± 0.4	9.5	2.90 ± 1.14	5.3 (×2.1/÷1.9)	6.9	1.3 ± 0.3	10.0	2.82 ± 1.60	4.5 (×2.2/÷1.9)
7.2	2.3 ± 0.6	10.0	2.57 ± 0.71	3.0 (×2.4/÷2.0)	7.3	1.9 ± 0.5	10.0	2.93 ± 1.43	5.2 (×2.1/÷1.8)
7.2	2.7 ± 0.7	10.0	2.40 ± 0.76	2.1 (×3.1/÷2.0)	7.3	3.7 ± 0.9	10.0	2.43 ± 1.19	2.3 (×3.4/÷2.0)
				RH = 60%					
7.5	1.9 ± 0.5	8.0	2.62 ± 0.73	4.2 (×2.3/÷2.0)	7.6	1.7 ± 0.4	9.0	3.39 ± 1.05	9.4 (×1.9/÷1.7)
7.5	1.3 ± 0.3	8.0	2.58 ± 1.10	3.9 (×2.6/÷2.0)	7.6	1.7 ± 0.4	9.0	3.31 ± 0.91	8.8 (×1.8/÷1.7)
7.5	1.9 ± 0.5	8.0	2.70 ± 0.69	4.8 (×2.2/÷1.9)	7.8	2.3 ± 0.6	8.5	3.10 ± 1.12	7.5 (×1.9/÷1.8)
7.5	2.1 ± 0.5	8.0	2.60 ± 0.61	4.0 (×2.2/÷2.0)	7.8	2.5 ± 0.6	8.5	3.04 ± 0.84	7.0 (×2.0/÷1.8)
7.6	1.7 ± 0.4	9.0	2.86 ± 0.87	5.3 (×2.1/÷1.8)	7.8	2.1 ± 0.5	8.5	2.93 ± 0.95	6.1 (×2.0/÷1.8)
7.6	2.0 ± 0.5	9.0	3.02 ± 0.97	6.5 (×2.0/÷1.8)	7.8	2.3 ± 0.6	8.5	2.63 ± 0.83	4.0 (×2.3/÷2.0)
				RH = 70%					
8.0	3.9 ± 1.0	8.5	3.12 ± 0.94	7.6 (×1.9/÷1.8)	7.5	2.4 ± 0.6	8.0	2.79 ± 0.91	5.4 (×2.1/÷1.9)
8.0	2.3 ± 0.6	8.5	3.14 ± 0.92	7.8 (×1.9/÷1.8)	7.4	2.4 ± 0.6	8.0	3.26 ± 0.97	9.4 (×1.9/÷1.7)
7.9	2.7 ± 0.7	8.5	2.72 ± 0.76	4.6 (×2.2/÷1.9)	6.7	1.9 ± 0.5	8.0	2.46 ± 0.52	3.0 (×2.7/÷2.0)
7.9	2.5 ± 0.6	8.5	3.34 ± 0.96	9.5 (×1.8/÷1.7)	7.1	1.6 ± 0.4	8.0	2.98 ± 0.78	6.9 (×2.0/÷1.8)
7.5	2.3 ± 0.6	8.0	3.32 ± 1.07	9.9 (×1.9/÷1.7)	7.1	2.3 ± 0.6	8.0	3.15 ± 0.91	8.4 (×2.2/÷1.7)
				RH = 80%					
7.8	3.9 ± 1.0	5.0	3.22 ± 0.91	14.4 (×1.9/÷1.7)	8.0	2.1 ± 0.5	5.0	3.29 ± 1.16	15.5 (×1.9/÷1.7)
7.8	3.6 ± 0.9	5.0	3.32 ± 1.08	15.9 (×1.9/÷1.7)	8.0	2.3 ± 0.6	5.0	3.22 ± 0.89	14.4 (×1.9/÷1.7)
7.9	3.0 ± 0.8	5.0	3.17 ± 1.05	13.7 (×1.9/÷1.7)	7.5	2.6 ± 0.7	5.0	2.79 ± 0.84	8.7 (×2.1/÷1.9)
7.9	2.4 ± 0.6	5.0	3.29 ± 1.08	15.5 (×1.9/÷1.7)	7.5	3.0 ± 0.8	5.0	2.42 ± 0.73	4.4 (×3.1/÷2.0)
8.0	2.1 ± 0.5	5.0	3.01 ± 1.02	11.5 (×2.0/÷1.8)	7.5	3.5 ± 0.9	5.0	3.31 ± 0.86	15.8 (×1.8/÷1.7)
8.0	2.4 ± 0.6	5.0	3.15 ± 1.13	13.4 (×2.0/÷1.8)	7.5	3.8 ± 1.0	5.0	2.79 ± 0.80	8.7 (×2.1/÷1.9)

[a] All of the experiments were conducted under conditions of $\bar{D}_p = 0.85 \pm 0.18$ μm, $[O/Ca]^{EDX}_{CaCO_3,t=0} = 2.0 \pm 0.5$ and $[O/Ca]^{EDX}_{Ca(NO_3)_2} = 5.5 \pm 1.0$. Uncertainty values represent one-standard deviation. k_I is the apparent, pseudo first-order rate constant determined from eq 4, and the uncertainty factors in the parentheses correspond to one standard deviation in $[O/Ca]^{EDX}_{CaCO_3,t}$, $[O/Ca]^{EDX}_{CaCO_3,t=0}$ and $[O/Ca]^{EDX}_{Ca(NO_3)_2}$.

by the substrate, values of k_I and thus γ_{net} would be underestimated. Hence, as discussed in our earlier publications,[28,29] a rigorous view is that the uptake coefficient reported here represents the lower limit.

The net uptake coefficient (γ_{net}) can be calculated by

$$\gamma_{net} = \frac{4k_I^*[CaCO_3]_{t=0}}{\bar{c}_{HNO_3}[HNO_3]_\infty}\frac{V_d}{S_d} = \frac{2[CaCO_3]_{t=0}\bar{D}_d}{3\bar{c}_{HNO_3}}\frac{k_I^*}{[HNO_3]_\infty} \quad (6)$$

where $[CaCO_3]_0 = 27.1$ M is a formal volume concentration of calcite particle, V_d/S_d is the particle volume-to-surface area ratio, $\bar{c}_{HNO_3} = 3.18 \times 10^4$ cm/s is the mean molecular speed of HNO_3 and $\bar{D}_d$ is the wet particle diameter at RH = 40%. The above equation is used in all subsequent analysis to obtain γ_{net} values. The determination of the droplet diameter required some special considerations. During the reaction, $CaCO_3$ is partially converted to hydrated $Ca(NO_3)_2$. At RH = 40%, $CaCO_3$ particles remain solid while $Ca(NO_3)_2$, a highly hygroscopic substance, rapidly

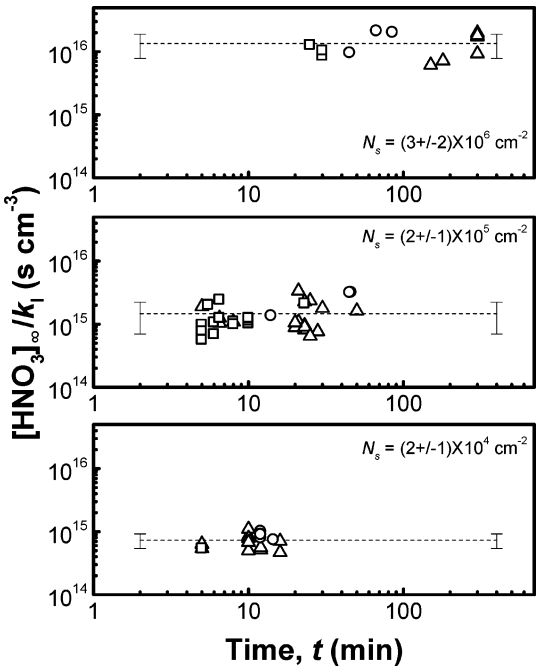

Figure 4. Variations of $[HNO_3]_\infty/k_I$ as a function of reaction time. Symbol are experimental data (Δ, 7.1 ± 0.4 ppb HNO_3; ○, at ∼14.4 ± 0.7 ppb; □, 24 ± 1.5 ppb). The dashed line indicates the average of the measured data; the error bars at the left- and rightmost of the line indicate one standard deviation of the $[HNO_3]_\infty/k_I$ data.

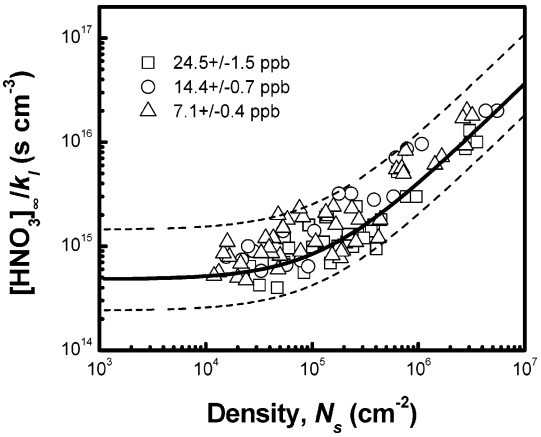

Figure 5. Experimental values of $[HNO_3]_\infty/k_I$, measured for ∼0.85 μm $CaCO_3$ particles under 40% RH as a function of particle number density N_s on the substrate surface. Symbols: experimental data for different concentrations of HNO_3 (Δ, 7.1 ± 0.4 ppb HNO_3; ○, at ∼14.4 ± 0.7 ppb; □, 24 ± 1.5 ppb), solid line: fit to data; dashed lines: the uncertainty of the fit.

takes up water, deliquesces, and undergoes hygroscopic growth. Under our experimental conditions, reacted particles are composed of a solid $CaCO_3$ core and a coating of concentrated aqueous solution of $Ca(NO_3)_2$ product. As the reaction proceeds and more of the $Ca(NO_3)_2$ product is formed, the particles undergo continuous growth, and as such the droplet diameter is expected to be larger than the dry particle diameter, $\bar{D}_d \geq \bar{D}_p$.

Therefore, the smallest size of the reacting particle can be approximated assuming $\bar{D}_{d,min} = \bar{D}_p = 0.85$ μm. Using this diameter value, we obtain $\gamma_{net} = 0.06$ (×3/÷2) for RH = 40%, which is somewhat lower than $\gamma_{net} = 0.11$ at RH = 33% reported for $CaCO_3$ particles by Vlasenko et al.[24] The largest size of the reacting particle ($\bar{D}_{d,max}$) can be estimated using a simplified core−shell model as described below. We assume

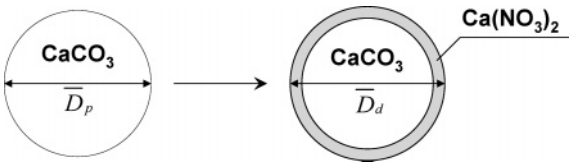

Figure 6. Simplified core−shell model for estimating the size of reacted $CaCO_3$.

that upon reaction a uniform coating of $Ca(NO_3)$ forms over a spherical $CaCO_3$ core, as illustrated in Figure 6. The volumes of the $CaCO_3$ core and the $Ca(NO_3)_2$ coating are given by eqs 7 and 8 as a function of reaction time, respectively

$$V_{CaCO_3,core}(t) = \frac{1}{6}\pi \bar{D}_p^{\,3}[1 - \chi(t)] \tag{7}$$

$$V_{Ca(NO_3)_2}(t) = \frac{4}{3}\pi(\bar{D}_p^{\,3} g_{Ca(NO_3)_2,RH})^3 \frac{\rho_{CaCO_3} MW_{Ca(NO_3)_2}}{\rho_{Ca(NO_3)_2} MW_{CaCO_3}} \chi(t) \tag{8}$$

where $\chi(t)$ is the extent of reaction, $g_{Ca(NO_3)_2,RH}$ the hygroscopic growth factor for $Ca(NO_3)_2$ at a specific relative humidity, and ρ and MW the mass density and molecular weight, respectively. If volume additivity is assumed, the largest diameter of a reacting $CaCO_3$ particle at the end of the experiment ($\bar{D}_{d,max}$) may be estimated by

$$\bar{D}_{d,max} = \left\{ \bar{D}_p^3[1 - \chi(t)] + (g_{Ca(NO_3)_2,RH}\bar{D}_p)^3 \frac{\rho_{CaCO_3} MW_{Ca(NO_3)_2}}{\rho_{Ca(NO_3)_2} MW_{CaCO_3}} \chi(t) \right\}^{1/3} \tag{9}$$

Here the extent of reaction is given by

$$\chi(t) = 1 - \frac{[CaCO_3]_t}{[CaCO_3]_{t=0}} \tag{10}$$

At a relative humidity of 40%, the hygroscopic growth factor for $Ca(NO_3)_2$ is $g_{Ca(NO_3)_2,RH\ =\ 40\%} = 1.4$.[33] The mass densities of pure $CaCO_3$ and $Ca(NO_3)_2$ were taken to be $\rho_{CaCO_3} = 2.71$ g/cm^3 and $\rho_{Ca(NO_3)_2} = 2.50$ g/cm^3.[37] It was found that under the current experimental conditions $\bar{D}_{d,max} \leq 1.2\bar{D}_p$ for RH = 40%. Toward higher RH values, the approximation yields larger differences in $\bar{D}_{d,max}$ values, i.e., $\bar{D}_{d,max} \leq 1.6\bar{D}_p$ at RH = 80%. Considering that these differences are notably smaller than the scatter in the data and that the k^*_I value represents the lower limit of reaction rates,[28,29] we used the $\bar{D}_{d,min} = \bar{D}_p$ approximation to calculate the uptake coefficients reported in this work, as tabulated in Table 1.

RH Dependence. To date, there is only one systematic investigation reported for nitric acid uptake onto a mineral dust surrogate, ATD, as a function of relative humidity.[24] Here we report the uptake coefficients of HNO_3 on $CaCO_3$ over a broad range of relative humidity. Experimental conditions and kinetic data for this series of the study are listed in Table 3. The uptake coefficients are summarized in Table 1.

Figure 7 shows uptake coefficients measured as a function of RH for $CaCO_3$ particles with a dry diameter of 0.85 μm. For comparison, data from Vlasenko et al.[24] and other previous measurements[16,21−23,38] are included in the figure. Additionally, the water adsorption isotherm measured on $CaCO_3$ particles at 296 K using a quartz crystal microbalance[39] and the water-to-solute ratios (WSR) measured[40] for dehydrating $Ca(NO_3)_2$ particles are also shown in the plot. The water uptake and WSR data are scaled to match the range of the γ_{net} values reported. As can be seen, the reactive uptake coefficient (γ_{net}) exhibits a

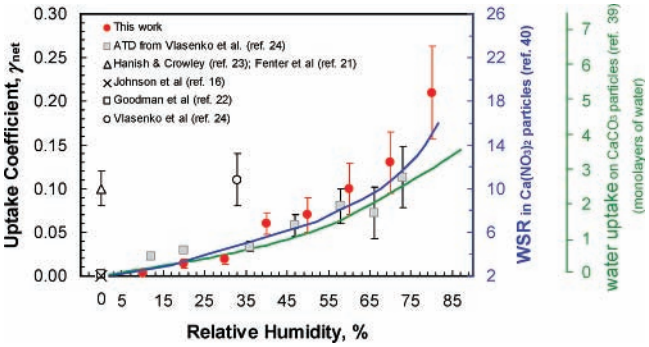

Figure 7. Experimentally determined uptake coefficient, γ_{net}, as a function of the relative humidity for HNO_3 reaction with $CaCO_3$. For comparison, literature data are also included. The green line indicates characteristic water uptake measured on $CaCO_3$ particles (ref 39). The blue line indicates characteristic water-to-solute ratio (WSR) measured in hydration experiments with levitated $Ca(NO_3)_2$ particles (ref 40). The water uptake and WSR data are scaled to match the reactive uptake coefficient (γ_{net}) values.

monotonic increase with increasing relative humidity from 0.032 at 10% RH to 0.21 at 80% RH, somewhat proportionally to the increase in the reported water uptake of $CaCO_3$ and $Ca(NO_3)_2$. Qualitatively, a similar effect of relative humidity has been reported for other heterogeneous reactions on solid surfaces including those of $CaCO_3$, ATD, borosilicate glass and some others.[22,26,34,41−43] The reaction enhancement observed under humid conditions is likely a combined result of several processes which play important roles in determining the overall reactivity of HNO_3 with $CaCO_3$, as discussed below.

It is generally understood that in the atmospheric environment the surface of calcium carbonate is terminated by hydroxyl (OH) and bicarbonate (CO_3H) groups ($Ca(OH)(CO_3H)$) due to the dissociative adsorption of water.[34] These terminal groups can be spectroscopically detected even under vacuum conditions.[36,44−47] The reaction between calcite and nitric acid is then initiated by exchange of bicarbonate ligand with nitrate to yield carbonic acid[36,45]

$$Ca(OH)(CO_3H) + HNO_3 \leftrightarrow Ca(OH)(NO_3) + H_2CO_3 \qquad (11)$$

Under dry conditions, the particle surface could be saturated with a layer of adsorbed carbonic acid, thus preventing further HNO_3 uptake. Surface saturation, however, is not an issue when RH is greater than 0%, as H_2CO_3 is unstable and rapidly dissociates into CO_2 and H_2O in the presence of water.[34,36] Additionally, the trace amount of water initially adsorbed at surface sites promotes the overall reaction by facilitating the dissociation of HNO_3 and enhancing ionic mobility for segregation or crystallization of nitrate at the surface and replenishment of $CaCO_3$ surface.[48] Similar water effects have also been observed in the studies of the heterogeneous reaction of dry NaCl crystals with nitric acid.[41,49−51]

As the amount of surface absorbed water increases at higher RH, acid assisted hydrolysis of the $CaCO_3$ surface is activated, which further facilitates the overall reaction[34]

$$HNO_3 \leftrightarrow H^+ + NO_3^- \qquad (12)$$

$$H^+ + CaCO_3 \leftrightarrow Ca^{2+} + HCO_3^- \qquad (13)$$

$$HCO_3^- + H^+ \leftrightarrow CO_2\uparrow + H_2O \qquad (14)$$

As the reaction proceeds, the highly hygroscopic $Ca(NO_3)_2$ product is formed on the surface of $CaCO_3$ particles, which deliquesces at 8−10% RH[19] and then undergoes subsequent hygroscopic growth at higher RH, similarly to the hygroscopic behavior of pure $Ca(NO_3)_2$ particles.[40] The presence of a large quantity of water at increasing RH facilitates hydrolysis reactions 12−14, but dissolution and a liquid layer also causes continued reactivity the carbonate surface, making more of the core of the particle available for the reaction. Eventually, these processes lead to the consumption of carbonate core. Although, Prince et al.[34] estimated that the viscosity of a metastable supersaturated nitrate product at low RH would be about 10^5 time larger than in pure water. Diffusion coefficients for dissolved species would substantially increase at higher RH; and characteristic diffusion times would be significantly shorter, which would have significant ramifications for the subsequent gas-to-particle chemistry. To conclude, all of the factors presented above enhance the reaction extent and may contribute to the observed increase in the uptake coefficient at higher RH.

The measured reactive uptake coefficients are in reasonable agreement with data reported for ATD, considering that our approach measures the lower limit for HNO_3 uptake on $CaCO_3$ particles. Additionally, the reactive uptake at low relative humidity determined here is consistent with the literature value of $(2 \pm 1) \times 10^{-3}$ and 2.7×10^{-3} at RH = 0% reported by Johnson et al.[16] and Santschi and Rossi,[52] respectively. The current results reported here at low relative humidity are, however, about a factor of 30 lower than values reported by Hanisch et al.[23] and Fenter et al.[21] The discrepancy is ascribed to the use of geometric surface area in the Knudsen cell experiments that contained many particle layers.[16]

In a previous NaCl study,[29] we investigated the effect of particle size on heterogeneous HNO_3 reactive uptake. A combined consideration of uptake coefficients reported in that[29] and previous works,[53,54] along with our modeling results,[29] indicated that the experimentally measured uptake coefficient (γ_{net}) of the HNO_3(gas)-to-NaCl(particle) reaction follows a characteristic rise-then-fall behavior with respect to particle size with the peak value of $\gamma_{net} \approx 0.2$, which occurs for 0.7 μm wet particles. The results showed that finite rate reaction kinetics is the major contributor to reactive uptake of HNO_3 onto small NaCl particles ($\bar{D}_d \ll 0.7$ μm) and gaseous diffusion of HNO_3 becomes a factor that limits its uptake onto larger NaCl particles ($\bar{D}_d \gg 0.7$ μm). Similarly, it is likely that the uptake of HNO_3 on 0.85 μm $CaCO_3$ particles might be also controlled by gas-phase HNO_3 diffusion. In this case, the experimentally measured reactive uptake coefficient (γ_{net}) cannot exceed the fundamental diffusion limit, which may be calculated as

$$\gamma_{net} \leq \Gamma_g = \frac{8D_{HNO_3-N_2}}{\bar{D}_d \bar{c}_{HNO_3}} \qquad (15)$$

Applying a size of the reacting particle in the range of $\bar{D}_p < \bar{D}_d < 1.6\bar{D}_p$ and a diffusion coefficient of $D_{HNO_3-N_2} = 0.118$ cm^2/s,[29] we obtain $\gamma_{net} \leq \Gamma_g = 0.22$ to 0.35. As seen in Figure 7, with the increase of RH our experimentally measured γ_{net} approaches this limit only at ~80% RH, while at lower RH the HNO_3-to-$CaCO_3$ reaction becomes increasingly kinetically controlled.

Conclusions and Atmospheric Implications

Heterogeneous reaction kinetics of gaseous nitric acid uptake on calcium carbonate particles were investigated experimentally using the PS-SFR approach. Two series of experiments were conducted at a fixed dry particle diameter $\bar{D}_p = 0.85$ μm with varying particle loading, HNO_3 concentration, and relative

humidity. The first series of experiments was performed for particles under 40% relative humidity. The results show that the variation of the apparent, pseudo first-order rate constant with particle loading and HNO_3 concentration is consistent with the pseudo first-order reaction assumption and a diffusion-kinetic analysis. Analysis yields the net reaction uptake coefficient $\gamma_{net} \geq 0.06(\times 3/\div 2)$ at 40% RH.

The second series of experiments examined the influence of relative humidity on the kinetics of HNO_3 uptake on $CaCO_3$ particles. The uptake was found to increase monotonically with an increase in relative humidity due to initial water absorption at the surface and subsequent $Ca(NO_3)_2$ hygroscopic growth. The reactive uptake coefficient is observed to jump between 10 and 20% RH, which is consistent with deliquescence of an amorphous $Ca(NO_3)_2$ hydrate in that RH range.

Mineral dusts have the largest atmospheric aerosol loading in terms of total mass, and their carbonate component is substantially reactive with gas-phase HNO_3,[19] leading to formation of hygroscopic $Ca(NO_3)_2$ containing particles in the atmosphere.[14] Under typical atmospheric conditions of RH > 20%, the $Ca(NO_3)_2$ reaction product, once formed, would remain in the aqueous phase throughout its atmospheric lifetime. This will significantly alter the physicochemical properties of the original aerosol particle in terms of light scattering and CCN activity.[55,56] In addition, heterogeneous reactions between HNO_3 and aerosol particles, such as $CaCO_3$ and NaCl, serve as major sinks for gaseous HNO_3 and nitrogen oxides, which impacts the overall chemical balance of the troposphere. Results from this work show that $CaCO_3$ has a similar reactive HNO_3 uptake to NaCl at RH = 40% but exhibits a very different humidity dependence. The uptake of HNO_3 onto NaCl was found to increase with the decreasing RH and peak around a relative humidity of 55%, and then below the efflorescence relative humidity (~45% RH) the uptake coefficient decreases rapidly.[29] As a result, if $CaCO_3$ and NaCl aerosol particles are present in the same HNO_3 polluted air mass, both heterogeneous reaction channels could occur.[13] They may take place equivalently or competitively depending on specific conditions.

Acknowledgment. The PNNL and the USC research groups acknowledge support provided by Tropospheric Chemistry and Radiation Sciences programs at the National Aeronautics and Space Administration (Grants NNG06GE89G and NNG06-GI51G). The UI research group acknowledges support provided by the National Science Foundation (Grant No. CHE-0503854). E.R.G. thanks the Department of Energy Global Change Education Program for support through a Graduate Research Environmental Fellowship. This work was performed at the William R. Wiley Environmental Molecular Sciences Laboratory, a national scientific user facility sponsored by the Department of Energy's Office of Biological and Environmental Research and located at Pacific Northwest National Laboratory (PNNL). PNNL is operated by the US Department of Energy by Battelle Memorial Institute under Contract No. DE-AC06-76RL0 1830. Finally, we thank Jennifer Schuttlefield of the University of Iowa for the quartz crystal microbalance water uptake measurements on $CaCO_3$.

References and Notes

(1) Ginoux, P.; Chin, M.; Tegen, I.; Prospero, J. M.; Holben, B.; Dubovik, O.; Lin, S. J. *J. Geophys. Res.-Atmos.* **2001**, *106*, 20255.

(2) Bauer, S. E.; Balkanski, Y.; Schulz, M.; Hauglustaine, D. A.; Dentener, F. *J. Geophys. Res.,-Atmos.* **2004**, *109*, Art. No. D02304, doi: 10.1029/2003JD003868.

(3) Bian, H. S.; Zender, C. S. *J. Geophys. Res.-Atmos.* **2003**, *108*, Art. No. 4672 doi:10.1029/2002JD003143.

(4) Tang, Y. H.; Carmichael, G. R.; Uno, I.; Woo, J. H.; Kurata, G.; Lefer, B.; Shetter, R. E.; Huang, H.; Anderson, B. E.; Avery, M. A.; Clarke, A. D.; Blake, D. R. *J. Geophys. Res.-Atmos.* **2003**, *108*, Art. No. 8824, doi:10.1029/2002JD003100.

(5) DeMott, P. J.; Cziczo, D. J.; Prenni, A. J.; Murphy, D. M.; Kreidenweis, S. M.; Thomson, D. S.; Borys, R.; Rogers, D. C. *Proc. Natl. Acad. Sci. U.S.A.* **2003**, *100*, 14655.

(6) Rudich, Y.; Khersonsky, O.; Rosenfeld, D. *Geophys. Res. Lett.* **2002**, *29*, Art. No. 4478, doi:10.1029/2002GL016055.

(7) Sokolik, I. N.; Toon, O. B. *J. Geophys. Res.-Atmos.* **1999**, *104*, 9423.

(8) Garrett, T. J.; Russell, L. M.; Ramaswamy, V.; Maria, S. F.; Huebert, B. J. *J. Geophys. Res.-Atmos.* **2003**, *108*, doi:10.1029/2002JD002228.

(9) Ravishankara, A. R. *Faraday Discuss.* **2005**, *130*, 9.

(10) Claquin, T.; Schulz, M.; Balkanski, Y. J. *J. Geophys. Res.-Atmos.* **1999**, *104*, 22243.

(11) Dentener, F. J.; Carmichael, G. R.; Zhang, Y.; Lelieveld, J.; Crutzen, P. J. *J. Geophys. Res.-Atmos.* **1996**, *101*, 22869.

(12) Song, C. H.; Carmichael, G. R. *J. Atmos. Chem.* **2001**, *40*, 1.

(13) Sullivan, R. C.; Guazzotti, S. A.; Sodeman, D. A.; Prather, K. A. *Atmos. Chem. Phys.* **2007**, *7*, 1213.

(14) Laskin, A.; Iedema, M. J.; Ichkovich, A.; Graber, E. R.; Taraniuk, I.; Rudich, Y. *Faraday Discuss.* **2005**, *130*, 453.

(15) Matsuki, A.; Iwasaka, Y.; Shi, G. Y.; Zhang, D. Z.; Trochkine, D.; Yamada, M.; Kim, Y. S.; Chen, B.; Nagatani, T.; Miyazawa, T.; Nagatani, M.; Nakata, H. *Geophys. Res. Lett.* **2005**, *32*, Art. No. L22806, doi:10.1029/2005GL024176.

(16) Johnson, E. R.; Sciegienka, J.; Carlos-Cuellar, S.; Grassian, V. H. *J. Phys. Chem. A* **2005**, *109*, 6901.

(17) Krueger, B. J.; Grassian, V. H.; Cowin, J. P.; Laskin, A. *Atmos. Environ.* **2004**, *38*, 6253. Erratum published in *Atmos. Environ.* **2005**, *39*, 395.

(18) Krueger, B. J.; Grassian, V. H.; Laskin, A.; Cowin, J. P. *Geophys. Res. Lett.* **2003**, *30*, Art. No. 1148, doi:10.1029/2002GL016563.

(19) Laskin, A.; Wietsma, T. W.; Krueger, B. J.; Grassian, V. H. *J. Geophys. Res.-Atmos.* **2005**, *110*, Art. No. D10208, doi:10.1029/2004JD005206.

(20) Liao, H.; Adams, P. J.; Chung, S. H.; Seinfeld, J. H.; Mickley, L. J.; Jacob, D. J. *J. Geophys. Res.-Atmos.* **2003**, *108*, Art. No. 4001, doi: 10.1029/2001JD001260.

(21) Fenter, F. F.; Caloz, F.; Rossi, M. J. *Atmos. Environ.* **1995**, *29*, 3365.

(22) Goodman, A. L.; Underwood, G. M.; Grassian, V. H. *J. Geophys. Res.-Atmos.* **2000**, *105*, 29053.

(23) Hanisch, F.; Crowley, J. N. *J. Phys. Chem. A* **2001**, *105*, 3096.

(24) Vlasenko, A.; Sjogren, S.; Weingartner, E.; Stemmler, K.; Gaggeler, H. W.; Ammann, M. *Atmos. Chem. Phys.* **2006**, *6*, 2147.

(25) Goodman, A. L.; Bernard, E. T.; Grassian, V. H. *J. Phys. Chem. A* **2001**, *105*, 6443.

(26) Maxwell-Meier, K.; Weber, R.; Song, C.; Orsini, D.; Ma, Y.; Carmichael, G. R.; Streets, D. G. *J. Geophys. Res.-Atmos.* **2004**, *109*, Art. No. D19S07, doi:10.1029/2003JD004464.

(27) Underwood, G. M.; Li, P.; Al-Abadleh, H.; Grassian, V. H. *J. Phys. Chem. A* **2001**, *105*, 6609.

(28) Laskin, A.; Wang, H.; Robertson, W. H.; Cowin, J. P.; Ezell, M. J.; Finlayson-Pitts, B. J. *J. Phys. Chem. A* **2006**, *110*, 10619.

(29) Liu, Y.; Cain, J. P.; Wang, H.; Laskin, A. *J. Phys. Chem. A* **2007**, *111*, 10026.

(30) Laskin, A.; Cowin, J. P.; Iedema, M. J. *J. Electron Spectrosc. Relat. Phenom.* **2006**, *150*, 260.

(31) Hua, Y. N. *J. Trace Microprobe Tech.* **2003**, *21*, 25.

(32) Hoffman, R. C.; Laskin, A.; Finlayson-Pitts, B. J. *J. Aerosol Sci.* **2004**, *35*, 869.

(33) Gibson, E. R.; Hudson, P. K.; Grassian, V. H. *J. Phys. Chem. A* **2006**, *110*, 11783.

(34) Prince, A. P.; Grassian, V. H.; Kleiber, P.; Young, M. A. *Phys. Chem. Chem. Phys.* **2007**, *9*, 622.

(35) Hering, S. V.; Lawson, D. R.; Allegrini, I.; Febo, A.; Perrino, C.; Possanzini, M.; Sickles, J. E.; Anlauf, K. G.; Wiebe, A.; Appel, B. R.; John, W.; Ondo, J.; Wall, S.; Braman, R. S.; Sutton, R.; Cass, G. R.; Solomon, P. A.; Eatough, D. J.; Eatough, N. L.; Ellis, E. C.; Grosjean, D.; Hicks, B. B.; Womack, J. D.; Horrocks, J.; Knapp, K. T.; Ellestad, T. G.; Paur, R. J.; Mitchell, W. J.; Pleasant, M.; Peake, E.; Maclean, A.; Pierson, W. R.; Brachaczek, W.; Schiff, H. I.; Mackay, G. I.; Spicer, C. W.; Stedman, D. H.; Winer, A. M.; Biermann, H. W.; Tuazon, E. C. *Atmos. Environ.* **1988**, *22*, 1519.

(36) Al-Hosney, H. A.; Grassian, V. H. *J. Am. Chem. Soc.* **2004**, *126*, 8068.

(37) Lide, D. R. *CRC Handbook of Chemistry and Physics*, 81 ed.; CRC Press: Boca Raton, FL, 2000.
(38) Underwood, G. M.; Li, P.; Usher, C. R.; Grassian, V. H. *J. Phys. Chem. A* **2000**, *104*, 819.
(39) Unpublished data. Measurements of water uptake on $CaCO_3$ particles using quartz crystal microbalance method reported in Schuttlefield, J.; Al-Hosney, H.; Zachariah, A.; Grassian, V.H. *Appl. Spectrosc.* **2007**, *61*, 283−292 and Schuttlefield, J., Ph.D. Dissertation, University of Iowa, **2008**.
(40) Tang, I. N.; Fung, K. H. *J. Chem. Phys.* **1997**, *106*, 1653.
(41) Davies, J. A.; Cox, R. A. *J. Phys. Chem. A* **1998**, *102*, 7631.
(42) Finlayson-Pitts, B. J.; Wingen, L. M.; Sumner, A. L.; Syomin, D.; Ramazan, K. A. *Phys. Chem. Chem. Phys.* **2003**, *5*, 223.
(43) Arens, F.; Gutzwiller, L.; Gaggeler, H. W.; Ammann, M. *Phys. Chem. Chem. Phys.* **2002**, *4*, 3684.
(44) Kuriyavar, S. I.; Vetrivel, R.; Hegde, S. G.; Ramaswamy, A. V.; Chakrabarty, D.; Mahapatra, S. *J. Mater. Chem.* **2000**, *10*, 1835.
(45) Al-Abadleh, H. A.; Al-Hosney, H. A.; Grassian, V. H. *J. Mol. Catal.* **2005**, *228*, 47.
(46) Stipp, S. L.; Hochella, M. F. *Geochim. Cosmochim. Acta* **1991**, *55*, 1723.
(47) Stipp, S. L. S. *Geochim. Cosmochim. Acta* **1999**, *63*, 3121.
(48) Al-Hosney, H. A.; Grassian, V. H. *Phys. Chem. Chem. Phys.* **2005**, *7*, 1266.
(49) Beichert, P.; Finlayson-Pitts, B. J. *J. Phys. Chem.* **1996**, *100*, 15218.
(50) Peters, S. J.; Ewing, G. E. *J. Phys. Chem. B* **1997**, *101*, 10880.
(51) De Haan, D. O.; Finlayson-Pitts, B. J. *J. Phys. Chem. A* **1997**, *101*, 9993.
(52) Santschi, C. and Rossi, M. J. *J. Phys. Chem. A* **2006**, *110*, 6789.
(53) Tolocka, M. P.; Saul, T. D.; Johnston, M. V. *J. Phys. Chem. A* **2004**, *108*, 2659.
(54) Saul, T. D.; Tolocka, M. P.; Johnston, M. V. *J. Phys. Chem. A* **2006**, *110*, 7614.
(55) Gibson, E. R.; Hudson, P. K.; Grassian, V. H. *Geophys. Res. Lett.* **2006**, *33*, Art. No. L13811, doi:10.1029/2006GL026386.
(56) Kelly, J. T.; Chuang, C. C.; Wexler, A. S. *Atmos. Environ.*, **2007**, *41*, 2904.